Advanced Engineering Materials

ADVANCED ENGINEERING MATERIALS
www.aem-journal.com

PERSPECTIVE OPEN ACCESS

Karl Popper and the Mechanisms of Hydrogen Embrittlement

H. K. D. H. Bhadeshia

School of Materials Science and Engineering, Queen Mary University of London, London, UK

Correspondence: H. K. D. H. Bhadeshia (hkdb@cam.ac.uk)

Received: 18 November 2025 | **Revised:** 5 May 2026 | **Accepted:** 12 May 2026

Keywords: falsifiablity | hydrogen embrittlement | Karl Popper | steels | theories of embrittlement

ABSTRACT

Small concentrations of hydrogen in a diffusible form within iron are well-established to harm the mechanical integrity of steels. There are theories that attempt to explain the pernicious role of hydrogen. The purpose here is to assess the models, in particular with respect to falsifiability and ability to predict any deterioration in properties or phenomena that can help mitigate hydrogen embrittlement.

1 | Introduction

This work focuses on the hydrogen embrittlement of steel, a field hampered by confusion and a lack of progress in both interpretation and the attribution of observations to specific theories. Inspired by Kragh's book [1], I scrutinise current hydrogen embrittlement models using the Popper falsifiability criterion. First, however, a clear definition of hydrogen embrittlement is necessary, as the concept is often over-generalised beyond the critical case of brittle fracture:

Consider a steel that does not yield discontinuously but at a proof strain of 0.002. Embrittlement corresponds to rapid crack propagation during failure in the elastic regime at a strain $\varepsilon_{\text{fracture}} < 0.002$. If the σ/ε curve exhibits discontinuous yielding, embrittlement manifests when $\sigma_{\text{fracture}} < \sigma_{\text{upper-yield}}$. Both cases represent entirely brittle and unstable fracture events.

Tests that involve substantial plasticity, such as those illustrated in Figure 1, can be misleadingly classified as hydrogen embrittlement. Misleading because uniform ductility is not compromised, and significant plastic strain precedes failure.

Such tests have questionable relevance to actual engineering service, where components operate well below the macroscopic yield strength. Furthermore, the calculated work of fracture during this failure mode ($\approx 1 \rightarrow 2\,\text{kJ m}^{-2}$) is three orders of magnitude greater than that associated with the perfect cleaving of an iron crystal.

In a brittle steel under stress control, cracks become unstable and advance rapidly once a critical stress intensity K_{IC} is reached. One could, therefore, classify the phenomenon illustrated in Figure 1 as a *benign* deterioration in ductility during testing at slow strain-rates that are inconsistent with catastrophic failure. Therefore, the focus here is on unstable crack propagation associated with sudden failure.

2 | Karl Popper

Popper's criterion of falsifiability [1, 3] emphasises that science must be capable of being disproven by observation or experiment. A theory is scientific if it makes 'risky predictions' that might be observed to be false. The statement 'only iron is magnetic' is falsifiable because observing a single other substance that is magnetic would disprove it.

Quantitative theories offer a greater degree of falsifiability because they propose precise, measurable relationships between

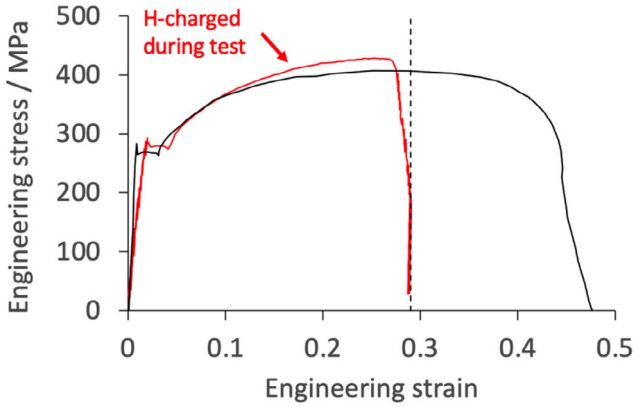

FIGURE 1 | Tensile tests ($\dot{\varepsilon} = 8.3 \times 10^{-6}\ s^{-1}$) on Fe–0.1C–2.03Mn wt% 1 mm thick sheet-steel containing a mixture of ferrite and pearlite. The dashed line reveals the plasticity ($\Delta\varepsilon_p \approx 0.02$) that persists after the engineering stress begins to collapse towards zero, over the stress range ≈400 → 200 MPa. Selected data from Okada et al. [2].

quantities. This allows for rigorous experiments that can either confirm or refute the theory (e.g., Einstein's prediction of starlight deflection by 1.75 arcsec [4, 5], or the known limits of Hooke's law [6] at high stress [7]). Science progresses by testing and attempting to refute bold conjectures.

In what follows, each theory for the hydrogen embrittlement of iron is assessed for falsifiability in the Popper sense, i.e., the ability to make credible predictions.

3 | Mechanism of Hydrogen Embrittlement

3.1 | Decohesion

Pfeil, in his experiments on pickled single- and poly-crystals of decarburised iron, observed both intra- and inter-granular fracture [8]. He concluded that hydrogen reduces the cohesion of the steel, though the elongation prior to macroscopically brittle failure was substantial, Figure 2.

Later work falsifies the idea of a loss of cohesion in iron caused by hydrogen, because the change in surface energy is simply too small to explain the dramatic reductions in toughness during brittle fracture (e.g. [9]). In Figure 3, the square root of the calculated ideal-cleavage surface energy is plotted because the fracture stress $\sigma_f \propto \sqrt{\gamma_s}$ according to the Griffith equation [10]. Often, cleavage even at cryogenic temperatures is not ideal but accompanied by highly-localised plasticity, in which case the Griffith equation is adapted by substituting an effective interfacial energy γ_p that in practice is at least seven times larger. Hydrogen does not readily segregate on $\{100\}_\alpha$ planes in intact ferrite crystals, and repulsion between hydrogen atoms limits the surface coverage to 0.25. At this maximum coverage, the surface energy γ_s is reduced marginally, yielding a maximum decrease in γ_s of 6%. Consequently, the theoretical fracture stress is minimally reduced, making the decohesion concept less credible.

These data cannot be used to estimate the reduction in tensile strength observed in Pfeil's experiments because those tests involved large elongations, which are inconsistent with a cleavage-based calculation. More fundamentally, the magnitude of the hydrogen-induced changes in surface energy is simply too small to explain any known observations on the loss of toughness in steels.

The decohesion theory nevertheless remains a popular interpretation of hydrogen embrittlement. To utilise it meaningfully, one could induce brittle failure in a steel (with specified defects and plane-strain conditions) by testing at a low enough temperature. The brittle-fracture stress (σ_f) would then be recorded across various dissolved hydrogen concentrations ([H]) and fitted empirically to the surface energy (γ_s) via $\sigma_f \propto \sqrt{\gamma_s}$. This empirical function could then be used to express the steel's quantitative sensitivity to hydrogen during brittle failure under defined conditions.

3.2 | High-Pressure Pores

The study of hydrogen embrittlement was in part stimulated by a troublesome defect that manifests during enamelling, whence the coating flakes as hydrogen accumulates at the coating/steel interface [11]. This led to the interpretation of blister formation on uncoated steel. In the early 1940s, before defect structures were established, it was hypothesised that internal 'disjunctions' in H-supersaturated steel could trap molecular hydrogen, creating immense aerostatic pressure that ultimately exceeded the steel's strength, thus explaining embrittlement.

Oriani [12] pointed out that the pressure developed within any bubble relies on a large hydrogen activity within the supersaturated steel, but in fact, the metal can embrittle even when in contact with gaseous hydrogen at a pressure of 0.1 MPa or less. This suggested that brittle failure of steels, induced by high-pressure internal-bubbles, is unlikely.

The pressure mechanism is prominent in intrinsically brittle materials like silicon. When implanted with hydrogen, molecular

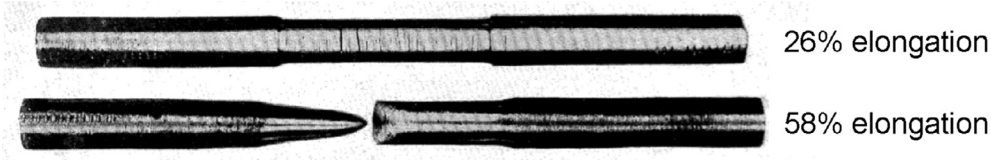

FIGURE 2 | A hydrogen-charged tensile test sample with 26% elongation prior to the development of fine cracks normal to the pulling direction, and one without hydrogen. Both samples are broken with the two halves placed in abutting positions. Reproduced and adapted from [8] (permission not required, https://royalsociety.org/journals/permissions/).

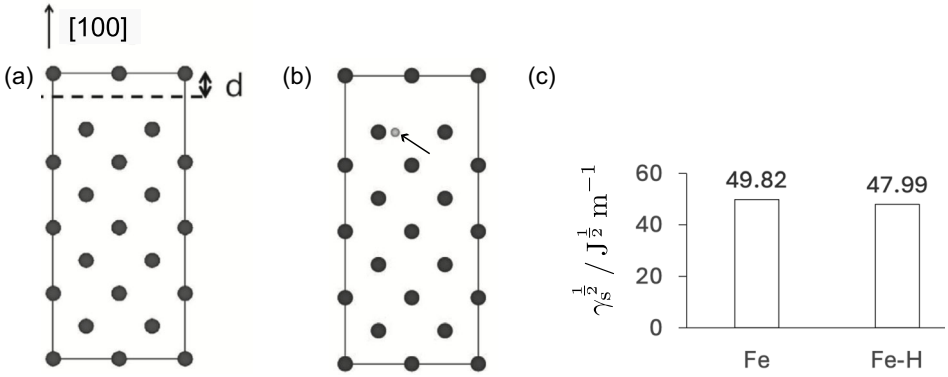

FIGURE 3 | Pure, ferromagnetic α-iron, 0 K. (a) Atomic structure for modelling {100} surface, with d representing a vacuum layer implemented to simulate cleavage. (b) The arrow identifies the location of a hydrogen atom in an octahedral interstice. The surface concentration of hydrogen is enormous, $H/(4Fe+H)=0.2$, since the problem is modelled as a $2\times2\times4$ supercell. (c) The calculated square-root of surface energy $\gamma_{s,\{100\}}$ assuming that the sample is ideally cleaved. The actual specific interfacial energies are 2.482 (Fe) and 2.303 J m^{-2} (Fe—H). After Song et al. [9].

H_2 enters its diamond lattice [13] and generates defects (Frenkel pairs and vacancy clusters). The clusters progressively fill with H_2 and reorganise into platelets on $\{100\}_{Si}$ or $\{111\}_{Si}$ planes. Continued H_2 accumulation increases the aerostatic pressure within these platelets, threatening the Si—Si bonds at the edges of the platelets, leading ultimately to oxidative cleavage via a reaction that forms silicon hydride:

$$\succ Si \underline{^{nH_2}} Si\leftarrow \quad \rightarrow \quad \succ Si-H \underline{^{(n-1)H_2}} H-Si\leftarrow \qquad (1)$$

where the silicon atoms are tetrahedrally bonded (symbol: $\succ Si-$).

Hydrogen implantation is used routinely to cleave (ion-cut) silicon via the bubble mechanism [14]. During annealing at 600°C, diffused hydrogen accumulates at existing H—H platelets (10–30 nm in size, predominantly on $\{100\}_{Si}$), forming bubbles that ultimately drive fracture. Failure also occurs on segments of $\{111\}_{Si}$, which roughens the fracture surface.

Although the deformation mechanisms of silicon differ dramatically from those of metallic iron, the pressure mechanism proposed by Zapffe and Sims in 1941 survives in a different incarnation. It has found a useful application in the production of silicon-on-insulator wafers for electronic devices. The calculated pressure inside the hydrogen bubbles in silicon is estimated at several gigapascals, which is sufficient to induce brittle fracture on specific crystallographic planes [15].

While extreme electrolytic hydrogen charging can cause blistering on uncoated iron, it is unclear if this pressure mechanism induces cleavage at the low hydrogen concentrations ($\approx$0.5 ppmw) that cause embrittlement in strong steels.

The falsifiability of this pressure-based interpretation can be tested quantitatively by the stress field around a pressurised spherical bubble of radius r_{bubble}:

$$\sigma_{radial}=-P\left(\frac{r_{bubble}}{r}\right)^3 \qquad \text{and} \qquad \sigma_{tangential}=\frac{P}{2}\left(\frac{r_{bubble}}{r}\right)^3$$

The tensile hoop stress ($\sigma_{tangential}$) is highly localised near the bubble interface. However, very small bubbles, which generate the highest pressure ($P\propto r_{bubble}^{-1}$), would be innocuous if their size is below the fracture mechanics critical crack size. Furthermore, molecular dynamics calculations [16] reaching high pressures (e.g., 3.5 GPa in nanovoids) are of dubious relevance, as the opening of a crack would immediately decrease the internal pressure, removing the sustained driving force for crack growth.

3.2.1 | Bubble/Hydride Hypothesis

A proposed two-stage hydrogen embrittlement mechanism during tensile testing [17] suggests that failure begins with rapid microscopic-cleavage (velocity >100 m s^{-1}) driven by the high-pressure of accumulated H_2 within internal cavities, causing hydride precipitation. This hydride suppresses dislocation emission at the crack tip, thus causing the initial microscopic-cleavage, but the resulting decline in hydrogen pressure should halt that crack. It is argued, however, that the initial high-velocity crack can continue propagating without the influence of hydrogen because its inertia suppresses bulk plasticity. It is not credible for the initial crack to advance unabated through the complex, fine-scale structures of martensitic or bainitic steels that were the subject of the original investigation. There exist countless crystallographic discontinuities within the structure of such steels.

The work also claims a 'disconnect' between ultimate tensile strength and fracture toughness in the context of hydrogen embrittlement, based on:

- The use of a threshold stress intensity K_{TH}, which represents the initiation limit for slow crack growth in hydrogen, rather than a plane-strain fracture toughness K_{IC}, which is the mechanical instability limit (the absolute ceiling of toughness).
- Failure in a hydrogen environment is not expected until the crack slowly grows from the K_{TH} threshold up to the critical fracture toughness in the environment K_{IC-H}. Thus, K_{TH} is a design parameter, not a true material property like K_{IC}. The estimated critical crack size based on K_{TH} therefore, incorrectly assumes immediate, catastrophic failure.

The blunt-notched tensile data [18] used in the analysis [17] exhibited ductility upon failure, not purely brittle elastic-regime failure predicted by the two-stage model. The strong '4340' steel was suggested to fail with zero ductility in this context, but this depends on microstructure: experiments reveal substantial ductility under similar conditions of 4340 yield strength and hydrogen concentration [19].

Diamond anvil cell experiments [20] show that the iron hydride necessary for this mechanism only forms at hydrostatic pressures of 3.5 GPa and decomposes at 2.2 GPa. This further limits the transient role of the hydride.

The model seems inconsistent with the true meaning of K_{TH} and K_{IC}, the former dealing with the stress-intensity required to initiate a crack that then grows slowly until a critical stress intensity is achieved. It does not align with experimental observations of ductility in strong steels subjected to hydrogen.

The particular susceptibility of strong steels to hydrogen is understood by established principles: greater barriers to dislocation emission at the crack tip and the ability of larger tolerable stresses to drive hydrogen diffusion towards regions where stress is concentrated [21, p. 319].

3.3 | Local Plastic Instability

Beachem [22] suggested that hydrogen concentrates in the triaxial stress field of a crack tip, which promotes severe, localised plastic deformation. This is akin to adiabatic shear [23], which has a different mechanism involving continuum phenomena, whereas any hydrogen-induced localised plasticity must consider the crystallography of slip and microstructure. The bulk material is said to remain strong because of its lesser, uniform hydrogen-content. The localisation results in a fracture surface that macroscopically appears brittle, but microscopically should be ductile. It should then be possible to detect the deformation debris at the fracture surface, extending to the depth of the hydrogen-enriched region, though the necessary degree of hydrogen enrichment is undefined.

This depth and its relation to the stress field at the crack tip have not been verified experimentally. It may define a quantitative Popper falsifiability criterion, if a model can be constructed that defines the expected depth.

The fracture-affected zone can be sectioned using a focused ion beam for high-resolution characterisation. It might even be possible to view the accumulation of hydrogen (immobilised by deformation defects) using atom probe tomography [24–26].

Crack velocity must be dampened by any accompanying plasticity. This could be monitored using acoustic emissions, which enable the detection of transient elastic waves generated by the rapid release of localised strain energy. Sudden brittle fracture typically generates distinct, large-amplitude acoustic signals, and an accelerating crack has a greater emission-event rate as it traverses diverse structures. Acoustic signals from ductile fracture reflect any irreversible energy dissipation. The technique primarily involves monitoring the frequency and amplitude (beyond threshold) of emissions, and the acoustic emission power [27]. This has been useful in interpreting proposed mechanisms of hydrogen embrittlement [28].

The concept of ideal cleavage (*cf.* pure silicon) is incompatible with the mechanism of localised plasticity. There is a lack of credible evidence to support hydrogen embrittlement by localised plasticity. Concerns regarding existing supporting arguments include:

1. Modelling: Current models lack the complexity required to accurately represent the problem.
2. In situ evidence: None exists for iron, only for nickel, which has a two orders of magnitude smaller Peierls barrier.
3. Fracture morphology: This is interpreted crudely in polycrystalline microstructures; experiments should instead focus on single crystals of iron.
4. Prediction: There is no quantitative prediction of the change in toughness caused by hydrogen via the local plasticity mechanism, for even the simplest of steels, rendering Popper falsification impossible.

3.3.1 | Dislocation Mobility

The proposition that dislocation mobility is enhanced by hydrogen in iron is based on in situ observations on nickel, where dislocations were observed to move more rapidly in the presence of hydrogen [29]. However, it is unsafe to extrapolate these findings to α-iron. The non-planar dislocation core in α-Fe is radically different from that in nickel, which has a Peierls barrier that is at least two orders of magnitude smaller than that of α-Fe [30]. No similar in situ observations exist for iron.

The mechanism requires the continuous enrichment of hydrogen in the vicinity of an advancing crack tip or in deforming regions. The hydrogen diffusion rate must be commensurate with the rate of deformation or crack advance. If the strain rate is too large, the hydrogen may not have sufficient time to replenish the regions ahead of the crack tip.

Referring to Table 1, the calculated diffusion distance in austenite is too small relative to the distance a crack must propagate to cause failure, thus ruling out the possibility of a large hydrogen concentration moving along with the crack tip during the test's duration. In contrast, the much faster diffusivity in ferrite means that hydrogen can in principle, keep up with an advancing crack provided the velocity is less than D_H^α/λ. Here λ is an interatomic spacing, so the ratio defines a maximum diffusion-velocity that can be compared against a proposed or measured rate of advance of a crack.

Slip localisation bears further scrutiny. When tested in high-pressure H_2 gas, the elongation of the ferritic sample in Figure 4a is reduced. Crucially, neither the yield nor the ultimate tensile strength is particularly affected by the hydrogen. This is counterintuitive if hydrogen enhances dislocation mobility. In any case, slip localisation cannot occur during the uniform elongation phase because maintaining continuity between differently oriented grains requires the simultaneous operation of at least five independent slip systems.

TABLE 1 | Calculations for a strain rate $\dot{\varepsilon} = 10^{-6}\,\mathrm{s}^{-1}$, plastic strain to failure of $\varepsilon_p^f = 0.3$, giving a time $t = \varepsilon_p^f/\dot{\varepsilon} = 3\times10^5$ s. The diffusion distance is taken as $\bar{z} \approx \sqrt{6D_H t}$. The gas constant $R = 8.3143\,\mathrm{J\,K^{-1}\,mol^{-1}}$. The diffusion data are from [31–33] and the temperature is set to 300 K. The interatomic spacing λ is taken to be 0.2 nm.

Phase	Diffusion coefficient D_H / $\mathrm{m^2\,s^{-1}}$	$\frac{D}{\lambda}$ / $\mathrm{m\,s^{-1}}$	$\bar{z}$ / m	Conclusion
γ	$2.5\times10^{-6}\exp\{-\frac{59300}{RT}\}$	6×10^{-7}	$\approx1.5\times10^{-5}$	Too small to move with the crack tip over the total fracture distance.
α	$\left(1.6^{+0.94}_{-0.59}\right)\times10^{-7}\exp\{-\frac{7076}{RT}\}$	47	0.12	Orders of magnitude faster, comparable to the self-diffusion of water.

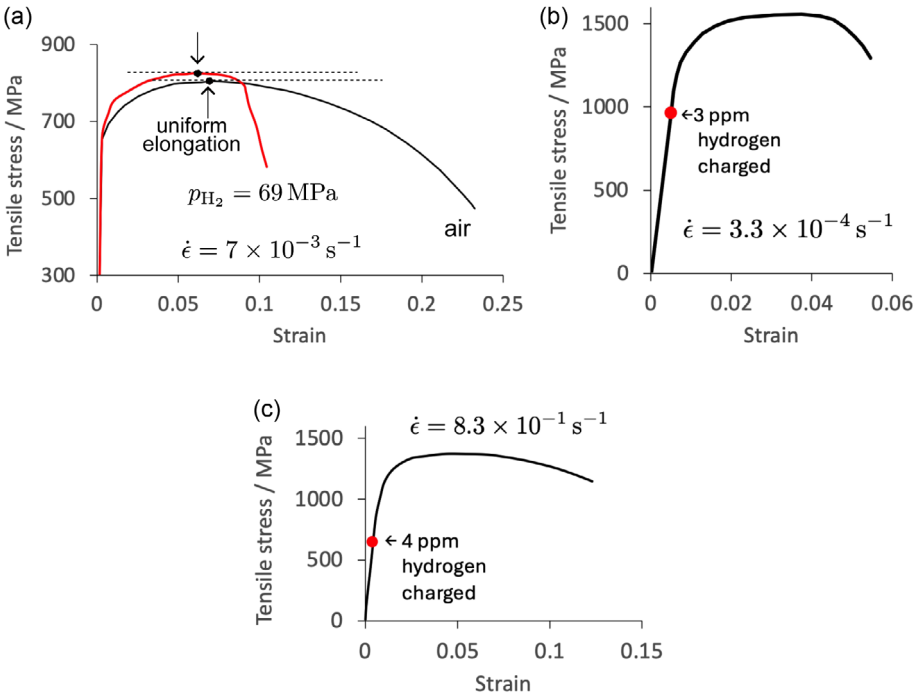

FIGURE 4 | (a) Engineering tensile-stress versus engineering-strain curves for a microalloyed Fe–0.064C–1.87Mn–0.1Si–0.47Ni–0.23Mo–0.035(Nb + V + Ti) wt% bainitic steel. The red curve represents testing with the sample exposed to high-pressure hydrogen. Selected data from Nanninga et al. [34]. (b) Ductile martensitic steel (Fe–0.24C–0.47Mn wt%) that fails within the elastic regime (red marker) when charged electrolytically with 3 ppm of hydrogen. Selected data from Ronevich et al. [35]. (c) High strain-rate tensile tests on martensitic Fe–0.2C wt% steel, both in the uncharged (curve) and hydrogen-charged (failed within elastic regime at red marker) conditions. Selected data from Momotani et al. [36].

Once necking and damage evolution begin, the hydrogen-exposed sample breaks prematurely. The final fracture is a mixture of a macroscopically ductile failure and a final brittle parting. Non-uniform elongation does not feature in most engineering designs where an application is not expected to undergo permanent deformation, except perhaps in crash scenarios where the total energy absorbed by the steel is important. It is not obvious why the non-uniform elongation component is missing in the hydrogen-charged specimen. The problem might be resolved by studying the evolution of damage during straining, either by sectioning a number of samples at different degrees of non-uniform elongation, or using X-ray tomography [37, 38, p. 95].

When cold-deformed and undeformed pearlitic steels are slow-rate tensile tested (both with and without electrolytically-charged hydrogen), the stress-plastic strain curves [26] are similar to those illustrated in Figure 4. Hydrogen exposure slightly reduces the uniform elongation and more significantly reduces the total elongation, resulting in a fracture that is a mixture of ductile and brittle components. Given the need for multiple slip systems during uniform elongation and the high dislocation density in the deformed samples, interpreting these results in terms of a localised plasticity model is not credible.

In stark contrast, other studies (Figure 4b) show that a hydrogen-charged sample can fail in the elastic regime of the stress–strain curve, which is correctly classified as brittle failure. This transition to brittle failure occurs when dealing with strong steels where the plastic zone at the crack tip will be limited, or when the strain rate is increased during tensile testing, Figure 4c [36].

These combined observations emphasise that the local plasticity model is a qualitative concept. It cannot estimate the ductile-brittle transition behaviour of steel as a function of temperature and strain rate. The model does not meet Popperian standards because

it lacks a quantitative structure that would make the underlying hypothesis susceptible to experimental disproof (falsification).

Assuming that local plasticity prevails, the following qualitative predictions designed to improve hydrogen resistance can be subjected to validation:

1. Promoting uniform deformation over localised deformation by enhancing the work-hardening rate. Increased work-hardening makes it more difficult for strain to localise into narrow bands. For example, this can be achieved by introducing transformation-induced plasticity within the microstructure.
2. Reducing the amount of diffusible hydrogen for a given total content by introducing hydrogen traps within the steel [39–43]. This mitigation method should lessen the effects of any embrittlement mechanism, as embrittlement is dependent on diffusible hydrogen.

3.4 | Blocking of Dislocation Emission

The original molecular dynamics simulations of hydrogen embrittlement by Song and Curtin [44, 45] provide insights into the mechanism of embrittlement and potentially, a quantitative framework for estimating susceptibility to hydrogen.

Without hydrogen, an increase in stress intensity from $0.8 \rightarrow 0.96$ MPa $\sqrt{\text{m}}$, causes the emission of a dislocation, the core of which is visible as cyan-coloured iron atoms in Figure 5a. The crack therefore, remains blunt.

When hydrogen is introduced, it migrates initially to the most favoured locations, which are the crack surfaces where the atoms congregate (Figure 5b). This is not relevant to crack behaviour because it occurs on already fractured surfaces, which, when saturated, permit dissolved hydrogen atoms to migrate instead towards regions of hydrostatic tension in the vicinity of the loaded crack tip. The threshold stress intensity required to emit dislocations from the crack tip increases in the presence of hydrogen, as evidenced by the lack of dislocation generation even at $K_{\text{I}} = 1.12$ MPa $\sqrt{\text{m}}$ (compared with 0.96 MPa $\sqrt{\text{m}}$ in the H-free sample). This obviously contradicts the idea that hydrogen enhances plasticity (Section 4.1).

The simulations further reveal the development of hydrogen-rich segments (shaded in Figure 5b), where the material has transformed from $\alpha \rightarrow \gamma$, forming a region that effectively blocks dislocation emissions.

As the hydrogen-enriched region grows, it interacts with the crack front, leading to the emission of a dislocation followed immediately by brittle cleavage (Figure 5c). This sequence is consistent with a ductile-to-brittle transition.

Song and Curtin assumed the existence of a pre-existing sharp crack, which, when loaded, was treated using linear, isotropic elasticity, based on stress field relations derived on the basis of Westergaard's work by Irwin, who had defined the meaning of stress intensity K_{I} [46, 47]. The coordinate axes are illustrated in Figure 5b. The z coordinate is parallel to the crack front, x to the growth direction, and y along the vertical to the crack face, in mode I loading under plane strain conditions. The primary interest is in calculating the hydrostatic tension at the crack tip, which drives the diffusion of hydrogen, so shear stresses are neglected.

$$\sigma_{xx} = \frac{K_{\text{I}}}{\sqrt{2\pi r}} \cos\left\{\frac{\theta}{2}\right\}\left[1 - \sin\left\{\frac{\theta}{2}\right\}\sin\left\{\frac{3\theta}{2}\right\}\right],$$

$$\sigma_{yy} = \frac{K_{\text{I}}}{\sqrt{2\pi r}} \cos\left\{\frac{\theta}{2}\right\}\left[1 + \sin\left\{\frac{\theta}{2}\right\}\sin\left\{\frac{3\theta}{2}\right\}\right],$$

$$\sigma_{zz} = \nu(\sigma_{xx} + \sigma_{yy}) = \frac{2\nu K_{\text{I}}}{\sqrt{2\pi r}} \cos\left\{\frac{\theta}{2}\right\}$$

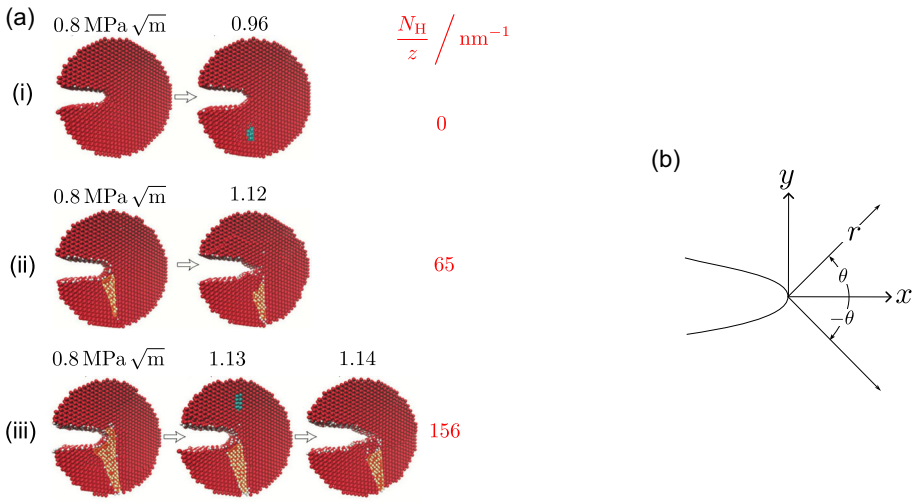

FIGURE 5 | (a) Simulated atomic configurations during mode I loading of a crack tip; stress intensities and the number of non-surface hydrogen atoms per unit length along the crack line N_{H}/z are indicated. Hydrogen atoms are coloured white, iron atoms red except those at dislocation cores which are cyan. The shaded regions correspond to locations of $\alpha \rightarrow \gamma$ transformation. (i) Hydrogen-free specimen simulation. (ii) Hydrogen introduced. (iii) The transition from ductile to brittle failure. Reprinted by permission from [45], Springer Nature. (b) Coordinate system around a sharp crack.

The hydrostatic tension in plane strain conditions is then:

$$\underbrace{\frac{\sigma_{xx}+\sigma_{yy}+\sigma_{zz}}{3}}_{\text{positive}} = \frac{2(1+\nu)K_{\mathrm{I}}}{3\sqrt{2\pi r}}\cos\left\{\frac{\theta}{2}\right\} \tag{2a}$$

Since σ_{ii} are all positive in Equation (2a), the term on the left causes a volume expansion at the crack tip, thus creating favourable space for hydrogen atoms to locate in.

The effect of stress on the chemical potential (μ_{H}) of hydrogen dissolved in α-iron was investigated by Bockris et al. [48]. Suppose that the activities of hydrogen in equilibrium with iron in the absence of stress, and when a stress is applied, are written as a_{H}^{0} and a_{H}^{σ} respectively, then the free energy G in the binary Fe—H system is given by

$$\begin{aligned} G\{\sigma=0\} &= \mu_{\mathrm{H}}^{0} + RT\ln\left\{a_{\mathrm{H}}^{0}\right\} + \mu_{\mathrm{Fe}}^{0} + RT\ln\left\{a_{\mathrm{Fe}}^{0}\right\} \\ G\{\sigma\} &= \mu_{\mathrm{H}}^{0} + RT\ln\left\{a_{\mathrm{H}}^{\sigma}\right\} + \mu_{\mathrm{Fe}}^{0} + RT\ln\left\{a_{\mathrm{Fe}}^{\sigma}\right\} \\ \Delta G = G\{\mp\sigma\} - G\{\sigma=0\} &\approx \pm RT\ln\left\{\frac{a_{\mathrm{H}}^{\sigma}}{a_{\mathrm{H}}^{0}}\right\} \approx \pm RT\ln\left\{\frac{c_{\mathrm{H}}^{\sigma}}{c_{\mathrm{H}}^{0}}\right\} \end{aligned} \tag{2b}$$

where $G\{\sigma\}$ refers to the free energy while the iron is stressed, and c refers to the concentration (fraction of hydrogen atoms per metal atom and $1-c$ for the iron). Since the amount of hydrogen is very small, it is reasonable to make the approximations that $a_{\mathrm{H}} \approx c_{\mathrm{H}}$, that the chemical potentials of the pure components μ^{0} do not change with σ and that $c_{\mathrm{Fe}} \approx 1$. The sign of ΔG will be negative when the stress is positive (tension) because the associated hydrostatic tension reduces the free energy of dissolved hydrogen, and vice versa. $G\{\mp\sigma\}$ can be written as a function of stress as follows:

$$\begin{aligned} G\{\mp\sigma\} &= G\{\sigma=0\} \pm |p|\Omega \\ \therefore \Delta G &= \pm|p|\Omega \end{aligned} \tag{2c}$$

where Ω the partial volume of hydrogen (how the presence of hydrogen affects the overall volume of α-iron) and p is the hydrostatic pressure, which is negative when it causes a volume expansion in iron, i.e., hydrostatic tension and the opposite for compression. For hydrostatic tension such as that at a crack tip subjected to mode I loading,

$$p\Omega = -\frac{\sigma_{xx}+\sigma_{yy}+\sigma_{zz}}{3}\Omega \tag{2d}$$

where the sign has been corrected from the chemical potential equation in [45]. The partial volume seems to depend both on temperature and the composition of the iron alloy. For iron at ambient temperature, it is $\approx 4.41\times10^{-30}\ \mathrm{m^3\ atom^{-1}}$ whereas for '4340' steel, the value is $\approx 3.25\times10^{-30}\ \mathrm{m^3\ atom^{-1}}$ [48]. Some calculations by Bockris [48] are instructive, where the stresses applied are uniaxial:

T, °C	Stress, MPa	$c_{\mathrm{H}}^{\sigma}/c_{\mathrm{H}}^{0}$	ΔG, J mol^{-1}
27	+118	1.047	−103
27	−118	0.961	+100

It is the gradient $\nabla\mu_{\mathrm{H}}$ that drives its diffusion. At a constant temperature,

$$(\nabla\mu_{\mathrm{H}})_r = -\nabla\left\{\frac{\sigma_{xx}+\sigma_{yy}+\sigma_{zz}}{3}\right\}\Omega \tag{2e}$$

$$= -\Omega\frac{(1+\nu)K_{\mathrm{I}}}{3(2\pi)^{\frac{1}{2}}r^{\frac{3}{2}}}\cos\left\{\frac{\theta}{2}\right\} \tag{2f}$$

The mean radial velocity of hydrogen atoms towards the crack tip is then

$$v_r = -\frac{\mathrm{d}r}{\mathrm{d}t} = -\frac{D_{\mathrm{H}}}{kT}(\nabla\mu_{\mathrm{H}})_r = \Omega\frac{D_{\mathrm{H}}(1+\nu)\dot{K}_{\mathrm{I}}t}{kT\,3(2\pi)^{\frac{1}{2}}r^{\frac{3}{2}}}\cos\left\{\frac{\theta}{2}\right\} \tag{2g}$$

where $\dot{K}_{\mathrm{I}}$ is the loading rate and t the time. At a time $t=t'$, all the hydrogen within a radius $r=r'$ can arrive at the crack tip,

$$\begin{aligned} \int_{r=0}^{r=r'} r^{\frac{3}{2}}\mathrm{d}r &= \Omega\frac{D_{\mathrm{H}}(1+\nu)\dot{K}_{\mathrm{I}}}{kT\,3(2\pi)^{\frac{1}{2}}}\cos\left\{\frac{\theta}{2}\right\}\int_{t=0}^{t=t'} t\,\mathrm{d}t \\ r' &= \left(\Omega\frac{5D_{\mathrm{H}}(1+\nu)\dot{K}_{\mathrm{I}}}{12kT\,(2\pi)^{\frac{1}{2}}}\cos\left\{\frac{\theta}{2}\right\}\right)^{\frac{2}{5}} \end{aligned} \tag{2h}$$

Define c_0 as the equilibrium number of hydrogen atoms per iron atom in the unstressed crystal, then the number per unit volume is $2c_0/a_\alpha^3$ where a_α is the lattice parameter of ferrite, the unit cell of which contains two iron atoms. The number N_{H}/z of hydrogen atoms per unit crack length that have diffused to the vicinity of the crack at time t' is therefore[1]

$$\begin{aligned} \frac{N_{\mathrm{H}}}{z} &= \frac{2c_0}{a_\alpha^3}\int_{-\pi}^{\pi}\frac{(r')^2}{2}\mathrm{d}\theta = \beta\left\{\frac{1}{2},\frac{9}{10}\right\}\frac{2c_0}{a_\alpha^3}\left(\Omega\frac{5D_{\mathrm{H}}(1+\nu)\dot{K}_{\mathrm{I}}}{12kT\,(2\pi)^{\frac{1}{2}}}t^2\right)^{\frac{4}{5}} \\ &\equiv \underbrace{\beta\left\{\frac{1}{2},\frac{9}{10}\right\}}_{\approx 2.13926}\frac{2c_0}{a_\alpha^3}\left(\frac{5\Omega D_{\mathrm{H}}(1+\nu)K_{\mathrm{I}}^2}{12kT\,(2\pi)^{\frac{1}{2}}\dot{K}_{\mathrm{I}}}\right)^{\frac{4}{5}} \\ &\equiv b_4 K_{\mathrm{I}}^{\frac{8}{5}} \quad \text{with} \quad b_4 = 2.13926\frac{2c_0}{a_\alpha^3}\left(\frac{5\Omega D_{\mathrm{H}}(1+\nu)}{12kT\,(2\pi)^{\frac{1}{2}}\dot{K}_{\mathrm{I}}}\right)^{\frac{4}{5}} \end{aligned} \tag{2i}$$

with the β function being the Euler integral of the first kind, a symmetrical function of two variables. As stated by Song and Curtin, b_4 is the overall parameter that controls the kinetics of hydrogen segregation at the crack due to loading, diffusion, concentration and temperature. They suggested that $b_4^* = 1.4\times10^{11}\ \mathrm{MPa^{-8/5}m^{-9/5}}$ is a critical value that divides brittle cleavage ($b_4 > b_4^*$) from ductile behaviour. This is because $b_4 > b_4^*$ represents a domain of high hydrogen content, fast diffusion and slow loading rates that permit the hydrogen to maintain a large concentration in the crack vicinity.

The theory is said to be 'parameter free'; Song and Curtin applied it to a range of iron alloys to determine, by comparison with b_4^*, whether the steel behaves in a brittle or ductile manner (Table 1, [49]). The inputs they used to calculate $\dot{K}_{\mathrm{I}}$ are not reasonable; the pre-existing sharp-crack size was assumed to correspond to the grain size, which was in the range of 11–100 μm—this is far too large for the steels examined. It is not clear what the 'grain size' used refers to because, for the martensitic or bainitic steels in their analysis, the plate thicknesses are much less than 1 μm. Their data refer to an estimate of the prior austenite grain size, which is not relevant in determining the pre-existing crack size

since each such grain contains myriads of ferrite grains in the form of plates of martensite or bainite. There is no evidence from structural studies that cracks 11μm size (Table 1, [49]) exist in manufactured AerMet 100 [50]; it is likely that the other steels examined also have gross overestimates of the pre-existing sharp crack size. The incorrect outcome is to render $\dot{K}_I$ unrealistically large.

Notice also that b_4^* itself is a fitting parameter that was assumed to be constant. It must, however, be different for circumstances other than those they studied, because if it truly is fixed, then a comparison of b_4 and b_4^* would lead to the conclusion from Equation (2i) that the material becomes more brittle as the test temperature is increased (!) because b_4 increases as $T \uparrow$.

It is nevertheless useful to know that the growth of a crack, which requires a continuing supply of hydrogen to the vicinity of the crack tip, is related specifically to:

$$\text{crack growth rate} \propto \frac{D_H}{T} K_I(c_0)^{5/4} \tag{2j}$$

It would be useful in the interests of maintaining allegiance to Popper to test whether the dependence on c_0 is correct, though the obvious difficulty is that brittle failure corresponds to rapid fracture, making it difficult to measure growth rates. The model of Song and Curtin may be regarded as defining a putative cause of hydrogen embrittlement. As Turok stated in another context, 'it is healthy for science to have rival theories, which are as different as possible. This helps clearly identify which critical tests—be they observational or mathematical/logical—will be the key to distinguishing the theories and proving some of them wrong' [1, p.207].

4 | Hydrogen Embrittlement of Stable Austenite

Austenitic steels that do not transform into martensite (ε or α') are not in general embrittled by hydrogen, for the following reasons:

- They generally are not strong and possess a large intrinsic ductility. All of the common austenitic steels have yield strengths <400 MPa and ductility ≈ 50% [51, p.86].
- The temperature dependence of strength is limited given the very small Peierls barrier at ambient temperatures [52].
- The diffusion of hydrogen into austenite is orders of magnitude slower than in ferrite, Table 1.

Any reduction in tensile elongation of such steels falls into the benign category (Section 2), in which the hydrogen-charged sample exhibits substantive elongation prior to failure, Figure 6. The fracture surfaces of embrittled samples often are characterised by dimples rather than facets [53]. There are rarely features akin to cleavage or fast fracture that could be regarded as unsafe. Although the observations often are attributed to one or more of the mechanisms described in Section 4, the role of the plasticity prior to fracture is neglected, as is the necessity for multiple slip systems to engage in a continuous polycrystalline system. Simplistic interpretations of slip localisation in a single crystal with a single-slip system active do not reflect reality (e.g., Figure 3 [57]).

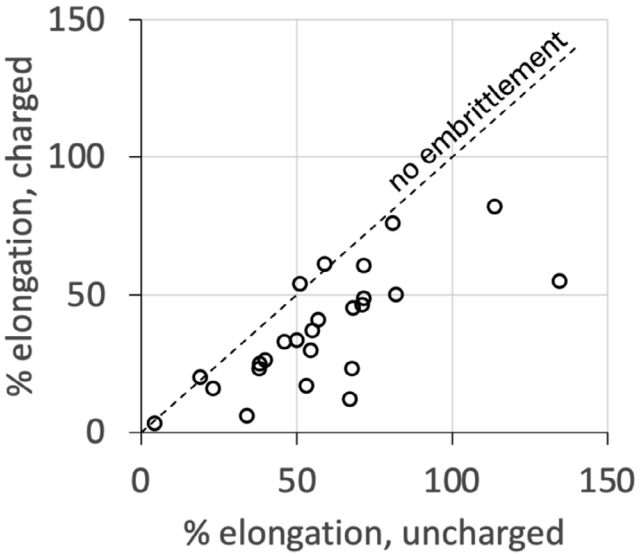

FIGURE 6 | Tensile ductility of stable austenitic steels before and after charging with hydrogen. The elongations plotted here do not include the strain recorded prior to yielding, whether that is due to elasticity in the sample or because of the lack of rigidity in the testing machine. Samples containing δ-ferrite are omitted. Data from [53–56].

4.1 | Mechanism of Benign Embrittlement

Hydrogen particularly reduces the non-uniform ductility in tension, presumably because it affects the formation and linkage of microscopic cavities that form, and there may be segments of the fracture surface that are work-hardened sufficiently to cleave. Closely spaced voids are able to link rapidly, causing early fracture. Transmission electron microscopy on thin crystals of 310 stainless steel under tension has shown that hydrogen charging causes the formation of minute voids that then caused cracking [58]. Hydrogen-free samples did not show this effect. This cracking mechanism is precisely described as hydrogen-induced void nucleation, growth, and connexion. Positron annihilation experiments further demonstrate that hydrogen enhances strain-induced vacancy formation in austenite, which is crucial for void nucleation [59].

In summary, hydrogen's role is to enhance the nucleation and growth of voids during plastic deformation, leading to their rapid linkage and a subsequent reduction in the steel's total ductility. The generation of tiny voids is attributed to the accumulation of both hydrogen and vacancies at inevitable stress concentrations in what is, after all, a heterogeneously deforming polycrystalline material while necking. Austenite in particular contains dissociated dislocations, which tend to pile up on the slip plane, so there will exist local stress concentrations within individual crystals in a polycrystalline sample.

It is believed that the binding between a hydrogen atom and a vacancy in austenite is favourable and stabilises the vacancy, although direct calculations or experiments are lacking. While an equilibrium concentration of vacancies exists due to their high entropy, the H-vacancy binding becomes relevant when excess vacancies are generated by plastic deformation. The agglomeration of these excess vacancies can lead to the formation of fine

voids [60].[2] Excess vacancies have also been demonstrated in hydrogenated, undeformed austenitic stainless steel by the characterisation of sessile dislocation loops (with Burgers vector $\frac{a_\gamma}{3}\langle 111\rangle_\gamma$), which are typical of quenched or irradiated steels containing a surplus of vacancies [61].

If the mechanism of embrittlement based on hydrogen/vacancy accumulation at stress concentrations is active, then increasing the stacking fault energy of the austenite would be beneficial. A higher stacking fault energy would avoid the dislocation pile-ups that create these stress concentrations. Recent work confirms the importance of the stacking fault energy, which satisfies the Popper falsifiability criterion for this mechanism [62].

When single crystals of austenite (Fe–26Cr–32Ni–3Mo wt%) are hydrogen-charged and tested at 300 K, the deformation mode changes from pure slip to a mixture of slip and twinning [63]. The stacking fault energy, measured via the triple junction method, decreases significantly from 65 to 20 mJ m^{-2}. This reduction changes the dislocation structure from cellular to planar and alters the orientation dependence of the critical resolved shear stress. While the exact significance of embrittlement is unclear, the onset of twinning may contribute to embrittlement if twins intersect (Table 2).

It follows that the loss of ductility in austenite (its 'benign embrittlement') is caused primarily by an increase in the number density of voids due to hydrogen-vacancy interactions. The loss is not related to shear localisation caused by increased dislocation mobility, because hydrogen diffuses too slowly in austenite to maintain a concentrated presence ahead of an advancing crack tip. Atom probe tomography shows that hydrogen is not associated with dislocations in deformed austenite due to its low mobility relative to dislocation velocity [53]. Furthermore, a mechanism relying on hydrogen reducing the shear modulus [68] is not relevant, as the average hydrogen concentration is only in parts per million, and any localised accumulation at a crack tip would still be limited by hydrogen's slow diffusion.

One way to falsify this hypothesis would be to increase the number density of hydrogen traps in austenite that compete with its association with vacancies.

4.2 | Predominantly Brittle Fracture of Stable Austenite

Nitrogen in austenite affects dislocation mobility, making screw dislocations sessile and edge dislocations less mobile [52]. This can cause brittle cleavage and induce a ductile–brittle transition in austenite as a function of temperature. It is therefore

TABLE 2 | Tensile tests on stable austenitic steels, some of which are charged with hydrogen. The engineering strain ϵ_p^f corresponds to fracture. The stacking fault energies are calculated thermodynamically using [Equation (1) [64]; where these energies were missing, they have kindly been calculated using this method, by Ehsan Ghassemali of Jönköping University via Steve Ooi of Ovaco. The embrittlement index is defined as $\%EI\{x\} = 100(x_{air} - x_H)/x_{air}$ where x = property measured. The results tabulated can vary with H-charging method; where multiple methods were applied, the worst scenario is assumed. The data may be sensitive to specimen sizes and shapes.

H	C	Mn	Cr	Al	Ni		SFE	ϵ_p^f	*%EI*	Ref.
	wt%	wt%	wt%	wt%	wt%	wt%	mJ m^{-2}			
No	0.21	30.9	—	1.1	—		19	0.56		[65]
Yes	”	”	”	”	”		”	0.20	64	[65]
No	0.45	24.5	—	4	—		24	1.13		[66]
Yes	”	”	”	”	”		”	0.82	27	[66]
No	0.49	24.0	4.04	—	—		29	0.43		[62]
Yes	”	”	”	”	”		”	0.13	70	[62]
No	0.21	30.9	—	1.1	—		29	0.37		[65]
Yes	”	”	”	”	”		”	0.12	67	[65]
No	0.05	0.95	18.2	—	8.1	0.47Si,0.14Mo	30	0.55		[67]
Yes	”	”	”	”	”	”	”	0.20	63	[67]
No	0.06	1.11	18.8	—	8.2		30	0.67		[59]
Yes	”	”	”	”	”		”	0.23	66	[59]
No	0.01	0.66	16.7	—	10.1	2.06Mo,0.041N,0.47Si	40	0.50		[67]
Yes	”	”	”	”	”	”	”	0.33	34	[67]
No	0.01	0.90	17.5	—	12.1	0.51Si,2Mo	40	0.59		[67]
Yes	”	”	”	”	”	”	”	0.61	0	[67]
No	0.25	30.4	2.71	1.75	3.0		49	0.34		[62]
Yes	”	”	”	”	”		”	0.38	0	[62]
No	1.10	18.73	5.02	6.00	—		66	0.85		[54]
Yes	”	”	”	”	”		”	0.79	7	[54]

interesting to investigate whether hydrogen exhibits a similar effect in nitrogen-alloyed stainless steels as it does in ferritic steels.

A nitrogen-containing austenitic steel tensile tested in a hydrogen environment showed a dramatic reduction in ductility, with plastic strain decreasing from 0.67 to 0.12. The fracture surface shifted from ductile to predominantly cleavage, Figure 7 [53].

Similar results were observed in an Fe–1C–31Mn–9Al wt% austenitic steel [53, 65]. While hydrogen causes hardening of the austenite, the precise mechanism for ductility reduction is unclear, with only speculation regarding localised plasticity [70]. Critically, there is no understanding of how this problem might be mitigated in the context of Popper's falsifiability criterion. An area for further research is understanding why hydrogen promotes intergranular fracture and whether refining the austenite grain size is beneficial, as explored in medium-manganese twinning-induced plasticity steels [71]. However, information on grain size refinement in such steels is contradictory, as hydrogen can suppress ε-martensite, which otherwise mitigates stress concentrations [72].

Hydrogen (specifically deuterium) tends to segregate at austenite grain boundaries but not at dislocations within the grain. Atom probe tomography on a hydrogen-charged and deformed Fe–26.9Mn–0.28C wt% steel showed deuterium segregated to the austenite grain boundary, peaking at about 1.4 ± 0.2 at.%. Deuterium did not segregate to the dislocations generated during deformation because its diffusion is too slow to remain in the rapidly moving strain field of dislocations, resulting in a random distribution of deuterium with grain interiors [53].

5 | Effect of Hydrogen on the Strength of Stable Austenite

Hydrogen causes solid solution hardening in austenite, which is consistent with its finite partial molar volume Ω causing a lattice parameter expansion [73]. Hydrogenation strengthens single crystals, reflected by an increase in the critical resolved shear stress (τ_{crss}), Figure 8a [63]. The nature of the deformation mechanism changes, making τ_{crss} orientation dependent (no longer a simple Schmid factor analysis). The hardening also manifests in polycrystalline steels, where the yield strength can double with the introduction of hydrogen. A yield point effect also appears in the stress–strain curve of hydrogenated polycrystalline samples, illustrated in Figure 8b [74].

Stress relaxation experiments on the same stainless steel indicated a relatively rapid decline in stress with time in the case of the hydrogen charged sample, following loading at constant displacement, Figure 9a [75]. This was interpreted as a reduction in the activation area A^*, which is the product of the length of the dislocation segment that is activated and the distance it moves forward. More formally, if the activation enthalpy for a dislocation to overcome an obstacle is G^*, then

$$A^* = -\left(\frac{\partial G^*}{\partial \tau^*}\right)_T \tag{3}$$

and τ^* is the effective shear stress. The logic in effect was that the hydrogen should increase the mobility of dislocations.

However, the interpretation is not strictly correct because the rate of stress relaxation depends on the level of applied

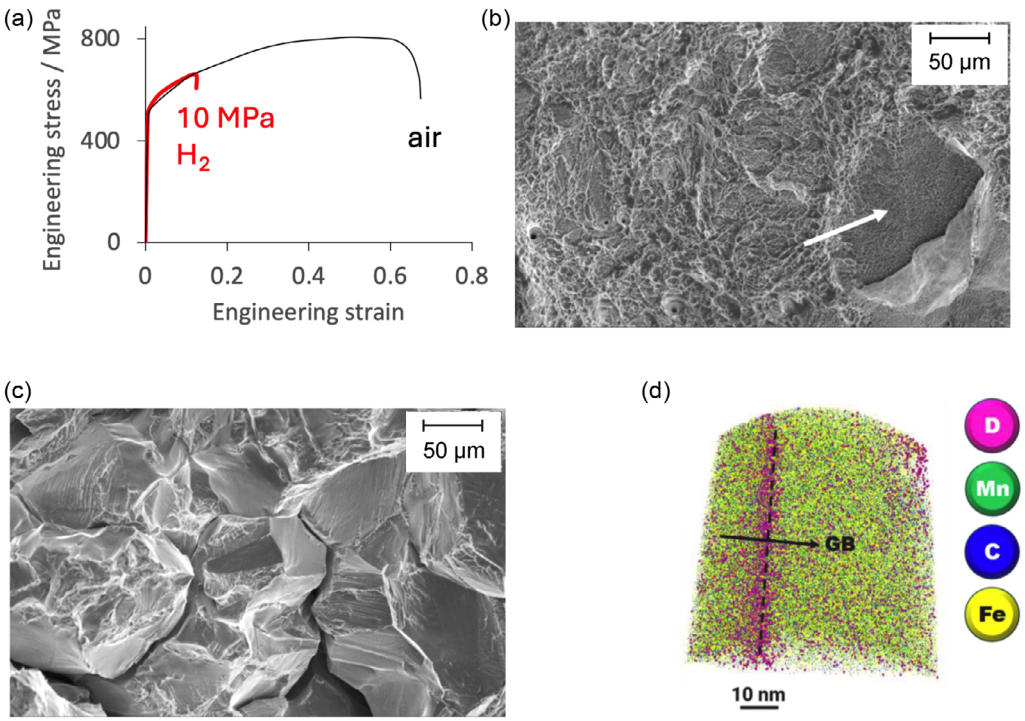

FIGURE 7 | Fe–18Cr–19Mn–0.8N wt% austenitic steel. (a) The effect of hydrogen on the σ/ϵ_p curve. (b) Fracture surface of the sample tested in air. The arrow points to a relatively flat region which has ductile dimples pockmarking the surface. (c) Mostly brittle cleavage and intergranular failure, in the sample tested in hydrogen. (d) Segregation of deuterium to an austenite grain boundary. Images reproduced from [53] and [69] with permission of Elsevier.

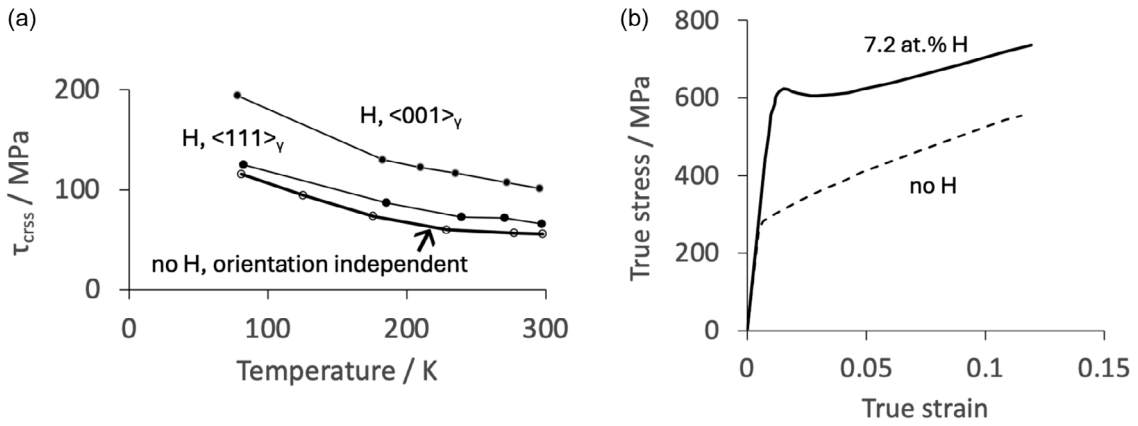

FIGURE 8 | (a) The measured critical resolved shear stress τ_{crss} of Fe–26Cr–32Ni–3Mo wt% single crystals, as a function of hydrogen, orientation and temperature. Selected data from Kireeva et al. [63]. The hydrogen not only enhances strength but also makes the response of the crystal anisotropic. (b) Slow strain-rate tensile stress/strain curves for polycrystalline Fe–0.018C–1.77Mn–0.67Si–25.37Cr–19.37Ni–0.4Mo–0.17Cu wt% austenitic stainless steel, with and without dissolved hydrogen. After Abraham an Altstetter [74].

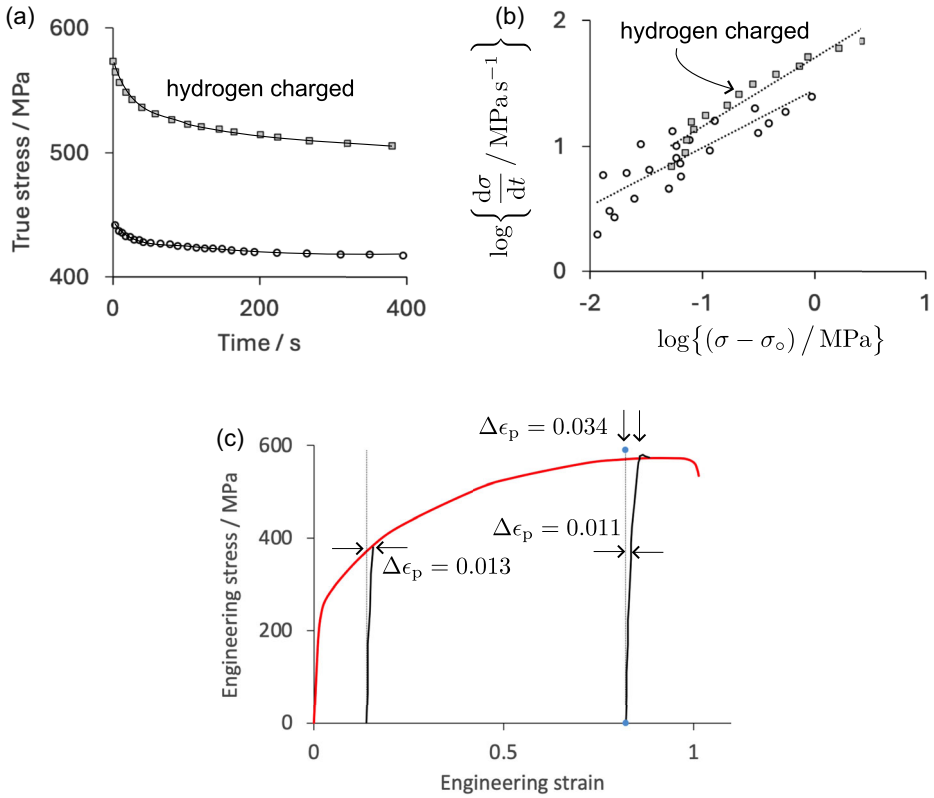

FIGURE 9 | (a) Stress relaxation tests on Fe–0.018C–1.77Mn–0.67Si–25.37Cr–19.37Ni–0.4Mo–0.17Cu wt% austenitic stainless steel with and without hydrogen. The points represent digitisation of curves in the original work [75]. (b) Analysis of the data in (a) using stress relaxation theory. The regression lines represent best-fit to the data. (c) Cyclic loading of Fe–0.07C–1.7Mn–8.9Ni–18.3Cr–0.2Mo–0.23Cu wt% stainless steel, not containing hydrogen. The dashed lines represent purely elastic deformation. Selected data from [76]; there were other loading/unloading cycles between the two illustrated, but omitted here for clarity. The red curve represents a continuous tensile test.

stress, which is much greater in the case of the hydrogenated sample [77]:

$$\frac{d\sigma}{dt} \propto (\sigma - \sigma^f)^{b_5} \tag{4}$$

where σ^f is the lattice friction stress, taken to be the asymptotic limit of each stress relaxation curve. Figure 9b show that the two sets of data show almost identical slopes, and there are even some regions of overlap. So the difference in the relaxation kinetics is not a reflection of an increase in dislocation mobility due to hydrogen, but rather that the velocity of dislocations depends on the applied stress, which is of a much greater magnitude in the hardened hydrogenated sample.

Abraham and Altstetter also noticed that when a tensile test was interrupted at $\sigma = \sigma_1$ in the plastic regime, and the load

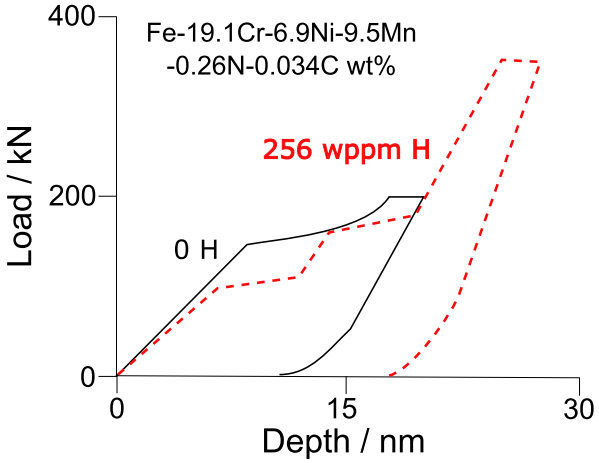

FIGURE 10 | Nanoindentation curves from a stable austenitic steel, adapted to represent the actual data presented in [78].

reduced to zero ($\sigma = 0$) before reloading, the recovery of stress applied stress to σ_1 was accompanied at the high stresses by what was described as microstrain, the magnitude of which was greater in the hydrogenated sample. This was again interpreted in terms of hydrogen, but there is a straightforward explanation.

Figure 9c illustrates a cyclic tension experiment on austenitic stainless steel that does not contain hydrogen. When pulled in tension, there are dislocation pile-ups, some of which are able to relax when the load is removed. These mobile dislocations therefore lower the yield stress when the sample is reloaded. A degree of plasticity is indicated by a deviation from the straight line representing elastic deformation, the difference is identified as $\Delta\varepsilon_p$. The magnitude of $\Delta\varepsilon_p$ is a function of the stress, so for both of the cycles illustrated, this 'microstrain' is almost identical at the same stress for the two cycles illustrated ($\sigma = 375$ MPa, $\Delta\varepsilon_p = 0.013 \approx 0.011$), but increases significantly to 0.034 at the larger stress of 573 MPa. One of the microstrains reported by Abrahams and Altstetter [75] for a hydrogenated sample was smaller at 0.0016 for $\sigma = 593$ MPa, proving that $\Delta\varepsilon_p$ cannot be attributed to hydrogen, but is simply an effect widely recognised in, for example, the Bauschinger effect without a stress reversal. Their observation of an apparent absence of $\Delta\varepsilon_p$ in the sample without hydrogen, is simply a reflection of its much smaller strength.

It seems appropriate to conclude that there is no evidence to support the hypothesis that hydrogen increases the mobility of dislocations in austenite, nor for the localisation of slip.

6 | Hydrogen and the Modulus

Nanoindentation of individual grains of austenite in the H-free and hydrogenated states (≈256 ppm) indicates that the Young's modulus decreases from 220 to 178 GPa due to hydrogen, Figure 10, while the hardness of the austenite increases by some 30%.

The experiments did not use the recommended repeated loading and unloading cycles, with each unloading terminated at 10% of the peak load in order to maintain continuous contact with the sample [79]. The penetration depth of the indenter into the hydrogenated sample is greater, creating larger slip steps on the surface. This would introduce more dislocations that are known to reduce the apparent stiffness by flexing and unflexing under load [80]. The evidence that the modulus is reduced by hydrogen is therefore weak. Indeed, there is no reduction in the stiffness of polycrystalline austenite by hydrogen; the elastic responses of the σ/ε curves for the H-free and hydrogenated states cannot be distinguished (Figures 7a and 8b).

There are first principles calculations of the elastic modulus of α-iron as a function of the concentration of its dissolved hydrogen. Small supercells are implemented to cope with computation times:

H, at%	H, wppm	Number of H atoms in supercell	Supercell dimensions
0.8	146	1	4 × 4 × 4
3.6	659	2	3 × 3 × 3

These hydrogen concentrations are orders of magnitude greater than the solubility of hydrogen in iron and exceed typical concentrations in exposed iron, Table 3.

The calculations therefore, lead to exaggerated interpretations with respect to the mechanism of embrittlement. This is illustrated in Figure 11, where there is a negligible change in shear modulus at realistic hydrogen concentrations. The concentration

TABLE 3 | Hydrogen content of steels exposed to the environment.

Location	Period	Measured Hydrogen/wppm	Note	Reference
Okinawa/Tsukuba	1999–2004	0.15	Stressed bolt	[81]
Okinawa/Tsukuba	1999–2004	0.16	Stressed bolt	[81]
Okinawa/Tsukuba	1999–2004	0.12	Stressed bolt	[81]
Okinawa/Tsukuba	1999–2004	0.11	Stressed bolt	[81]
Acidic soil, 2.5 *pH*	360 days	2.9	Unstressed corrosion	[82]
Acidic soil, 5.0 *pH*	360 days	3	Unstressed corrosion	[82]
Boiler fuel, no water	1050 h	0.07–0.12	Ship-engine steel	[83]
Engine oil, 0.01% water	1050 h	1.8–4.7	Ship-engine steel	[83]

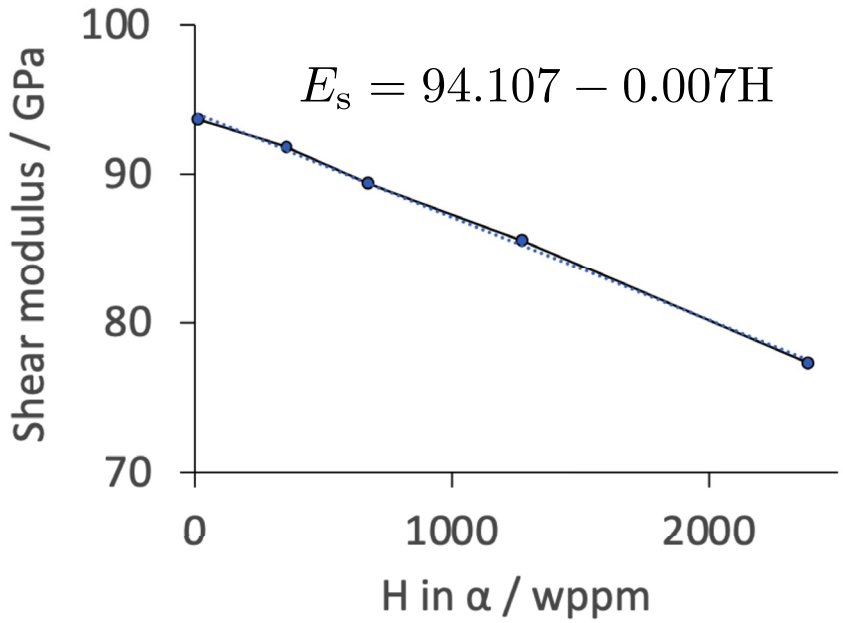

FIGURE 11 | First principles calculations showing the dependence of the shear modulus at 0 K of α-iron as a function of interstitially-dissolved hydrogen. The equation is obtained by best-fit linear regression to the data and shows that the change in E_s is negligible at a concentration of 1 wppm, which is typical in practice. Selected data from [84].

can, of course, be enhanced by stress triaxialities, but Equation (2b) indicates that for a hydrostatic tension of 400 MPa at 300 K, the ratio c_H^σ/c_H^0 is just 1.5. Resonance experiments show that an average concentration of $c_H^0 = 7 \rightarrow 8$ ppmw does not influence the Young's modulus of iron [85].

The modulus-based hydrogen effect does not address the extent of embrittlement to be expected nor the nature of the failure, so it fails the Popper falsifiability criterion.

7 | Conclusions

There clearly is a dire need to formulate quantitative models that enable engineering design as a function of the specific levels of hydrogen concentration expected to enter steel in the circumstances of application. The obvious way forward is to focus on fracture toughness determinations (K_{IC}) as a function of [H], and express the data empirically in terms of the effective cleavage surface energy. This is analogous exactly to the current practice for plane-strain conditions, where

$$K_{IC}^2 = \frac{2\gamma_p E}{1-\nu^2} \tag{5}$$

where γ_p is an effective surface energy that accounts for the some level of localised plasticity, E is the Young's modulus, and ν is the Poisson's ratio. The K_{IC} can then be used in engineering design so in that sense represent material properties.

The true surface energy γ is the purely thermodynamic energy required to break the atomic bonds across a plane to create two new, stress-free surfaces. For iron this would be between $2.3 \rightarrow 2.5\,J\,m^{-2}$ for $\{100\}_\alpha$, $\{110\}_\alpha$ and $\{111\}_\alpha$ surfaces [86]. Failure in this way would represent a process in which no energy is dissipated through other mechanisms. The effective surface energy γ_p accounts for all the energy dissipated from the crack tip per unit area of crack advance, primarily the localised plastic work per unit area, w_p, associated with a finite plastic zone at the crack tip, $\gamma_p = \gamma + w_p$ that can be much larger. And yet, the effective surface energy is able to function semi-empirically as a parameter is safe design against rapid fracture when hydrogen is not present in the steel. There is no reason why such an approach cannot be exploited for hydrogenated steel.

This approach clearly relies on hydrogen affecting the fracture-surface energy so it has similarities to the original thinking on decohesion, Section 4.1. The caveat is that the K_{IC} tests can be rigorous representations of potential reductions in toughness due to hydrogen. They can be used in engineering design, and unlike most assessments based on tensile tests, they represent unstable crack propagation. The function $K_{IC} = f\{[H]\}$ can in principle even be applied to estimate the safe-life of a component subjected to fatigue crack growth.

Once the dependence $K_{IC} = f\{[H]\}$ is established, the quantitative variation in γ_p with hydrogen can potentially provide imaginative, though hopefully falsifiable, fodder for further investigations. If this hypothesis is accepted, then the following become less relevant:

1. Tensile tests that are associated with benign embrittlement, accompanied by substantial plasticity. Such tests do not represent phenomena such as the catastrophic fracture of pressure vessels.
2. The routine interpretation of rudimentary embrittlement experiments with respect to unfalsifiable hydrogen embrittlement models.

One aspect not covered here, due to time limitations, is the widespread application of Sievert's law to estimate the atomic hydrogen concentration within a steel due to pressure from molecular hydrogen gas. This is in the context of the imminent use of existing pipelines designed for fossil gas, to transmit hydrogen. Sievert's law [87, 88] is assumed without adequate attention to the need for hydrogen dissociation at the steel surface. Johnson pointed out in 1988 that there are surface impedances such as oxides, which hinder hydrogen entry and exit form the steel at ambient temperatures [89]. A palladium sputter-coating leads to Sievert's law behaviour, whereas the square root dependence on pressure is unlikely to be justified otherwise.

Nomenclature

Symbols

α	Ferrite or α-iron
$\gamma_{s,\{100\}}$	Surface energy of plane with Miller indices {100}
γ	Austenite
$\dot{\varepsilon}$	Strain rate
$\varepsilon_{\text{fracture}}$	Strain when fracture occurs in the elastic regime
ε_{p}	Plastic strain
θ	Angular coordinate
λ	Interatomic spacing
μ_{H}	Chemical potential of hydrogen
ν	Poisson's ratio
Ω	Partial volume of hydrogen
σ_{radial}	Radial stress
$\sigma_{\text{tangential}}$	Tangential stress
$\sigma_{0.002}$	Proof strength
σ_{f}	Brittle fracture stress
$\sigma_{\text{upper}-\text{yield}}$	Upper yield stress during discontinuous yielding.
τ^*	Effective shear stress
τ_{crss}	Critical resolved shear stress
a_α	Lattice parameter of ferrite
a_{H}	Activity of hydrogen
A^*	Activation area
b_i	Empirical constants
c_0	Number of H atoms per Fe atom in unstressed crystal
c_{H}	Concentration of hydrogen
E	Young's modulus
E_{s}	Shear modulus
EI	Embrittlement index
G	Free energy
G^*	Activation free energy
k	Boltzmann constant
$\dot{K}_{\text{I}}$	Rate of loading to a particular stress intensity
$K_{\text{IC}-\text{H}}$	Critical fracture toughness in environment with hydrogen
K_{IC}	Fracture toughness in mode I loading
K_{I}	Stress intensity in general
K_{TH}	Threshold stress intensity
N_{H}	Number of hydrogen atoms
P	Pressure
r	Radial coordinate
r_{bubble}	Bubble radius
R	Gas constant
SFE	Stacking fault energy
t	Time
T	Temperature
v_r	Radial velocity of hydrogen
w_{p}	Work done per unit area
z	Hydrogen diffusion distance, or cartesian coordinate
D_{H}	Hydrogen diffusion coefficient

Author Contributions

H. K. D. H. Bhadeshia: conceptualisation (lead), writing – original draft (lead), writing – review & editing (lead).

Funding

The authors have nothing to report.

Conflicts of Interest

The author declares no conflicts of interest.

Data Availability Statement

Data sharing is not applicable to this article as no new data were created or analysed in this study.

Endnotes

[1]Since $\cos\{-\theta/2\} = \cos\{\theta/2\}$, its integral between the limits $-\pi, +\pi$ is equivalent to twice its integral between the limits $0, \pi$.

[2]Although the role of martensite, detected using X-ray diffraction, seems to have been neglected.

References

1. H. Kragh, *Higher Speculations: Grand Theories and Failed Revolutions in Physics and Cosmology: Oxford* (Oxford University Press, 2011).

2. K. Okada, A. Shibata, Y. Takeda, and N. Tsuji, "Crystallographic Feature of Hydrogen-Related Fracture in 2Mn-0.1 C Ferritic Steel," *International Journal of Hydrogen Energy* 43 (2018): 11298–11306.

3. K. R. Popper, *Logik der Forcschung (the Logic of Scientific Discovery): Vienna* (Verlag von Julius Springer (English edition 1959), 1935).

4. A. Einstein, "Die Feldgleichungen der Gravitation," *Sitzungsberichte der Königlich Preußischen Akademie der Wissenschaften* 25 (1915): 844–847.

5. F. W. Dyson, A. S. Eddington, and C. Davidson, "IX. a Determination of the Deflection of Light by the Suns Gravitational Field, from Observations Made at the Total Eclipse of May 29, 1919," *Philosophical Transactions of the Royal Society of London. Series A, Containing Papers of a Mathematical or Physical Character* 220 (1920): 291–333.

6. R. Hooke, *De Potentia Restitutiva, or of Spring. Explaining the Power of Springing Bodies* (Royal Society, 1678).

7. H. K. D. H. Bhadeshia, "High-Strength Steels," in *Future Developments of Metals and Ceramics*, ed. J. A. Charles, G. W. Greenwood and G. C. Smith (Institute of Materials, 1992), 25–74.

8. L. B. Pfeil, "The Effect of Occluded Hydrogen on the Tensile Strength of Iron," *Proceedings of the Royal Society of London. Series A, Containing Papers of a Mathematical and Physical Character* 112 (1926): 182–195.

9. E. J. Song, H. K. D. H. Bhadeshia, and D.-W. Suh, "Effect of Hydrogen on the Surface Energy of Ferrite and Austenite," *Corrosion Science* 77 (2013a): 379–384.

10. A. A. Griffith, "The Phenomena of Rupture and Flow in Solids," *Philosophical Transactions of the Royal Society A* 221 (1921): 163–197.

11. C. Zapffe and C. Sims, "The Relation of Defects in Enamel Coatings to Hydrogen in Steel," *Journal of the American Ceramic Society* 23 (1940): 187–219.

12. R. Oriani, "Hydrogen Embrittlement of Steels," *Annual Review of Materials Science* 8 (1978): 327–357.

13. G. Cerofolini, F. Corni, S. Frabboni, C. Nobili, G. Ottaviani, and R. Tonini, "Hydrogen and Helium Bubbles in Silicon," *Materials Science and Engineering: R: Reports* 27 (2000): 1–52.

14. T. Hochbauert, A. Misra, R. Verda, et al., "Hydrogen-Implantation Induced Silicon Surface Layer Exfoliation," *Philosophical Magazine B* 80 (2000): 1921–1931.

15. X. Lu, N. W. Cheung, M. D. Strathman, P. K. Chu, and B. Doyle, "Hydrogen Induced Silicon Surface Layer Cleavage," *Applied Physics Letters* 71 (1997): 1804–1806.

16. X. Li, W. Huang, X. Wu, et al., "Effect of Hydrogen Charging Time on Hydrogen Blister and Hydrogen-Induced Cracking of Pure Iron," *Corrosion Science* 181 (2021): 109200.

17. S. S. Shishvan, G. Csányi, and V. S. Deshpande, "Hydrogen Induced Fast-Fracture," *Journal of the Mechanics and Physics of Solids* 134 (2020): 103740.

18. C. W. San Marchi and B. P. Somerday, *Technical Reference for Hydrogen Compatibility of Materials* Sandia National Laboratories, (2012), Technical Report SAND2012-7321.

19. I.-O. Shim and J. Byrne, "A Study of Hydrogen Embrittlement in 4340 Steel I: Mechanical Aspects," *Materials Science and Engineering: A* 123 (1990): 169–180.

20. M. Tkacz, "Thermodynamic Properties of Iron Hydride," *Journal of Alloys and Compounds* 330 (2002): 25–28.

21. H. K. D. H. Bhadeshia and K. R.W., *Honeycombe: Steels – Structure, Properties and Design*, 5th ed. (Elsevier Butterworth-Heinemann, 2024).

22. C. D. Beachem, "A New Model for Hydrogen-Assisted Cracking (hydrogen "Embrittlement," *Metallurgical Transactions* 3 (1972): 437–451.

23. M. E. Backman and S. A. Finnegan, "The Propagation of Adiabatic Shear," in *Metallurgical Effects at High Strain Rates*, ed. R. W. Rhode, B. M. Butcher, J. R. Holland, and C. H. Karnes (Plenum Press, 1973), 531–543.

24. J. Takahashi, K. Kawakami, and T. Tarui, "Direct Observation of Hydrogen-Trapping Sites in Vanadium Carbide Precipitation Steel by Atom Probe Tomography," *Scripta Materialia* 67 (2012): 213–216.

25. S. Jakob, M. Thuvander, and S. W. Ooi, "Comparison of Hydrogen Resilience of Three Different Corrosion-Resistant Martensitic Steels," *Materials & Design* 252 (2025): 113747.

26. C. Huang, C. Cui, R. Niu, et al., "Strong Hydrogen Trapping by Tangled Dislocations in Cold-Drawn Pearlitic Steels," *Acta Materialia* 296 (2025): 121231.

27. H. Wadley, C. Scruby, and J. Speake, "Acoustic Emission for Physical Examination of Metals," *International Metals Reviews* 25 (1980): 41–64.

28. H. Dunegan and A. Tetelman, "Non-Destructive Characterization of Hydrogen-Embrittlement Cracking by Acoustic Emission Techniques," *Engineering Fracture Mechanics* 2 (1971): 387–402.

29. I. Robertson and H. Birnbaum, "An HVEM Study of Hydrogen Effects on the Deformation and Fracture of Nickel," *Acta Metallurgica* 34 (1986): 353–366.

30. Y. Si, Y. Zhang, D. Chen, et al., "Atomistic Determination of Peierls Barriers of Dislocation Glide in Nickel," *Journal of the Mechanics and Physics of Solids* 178 (2023): 105359.

31. F. R. Coe, *Welding Steels without Hydrogen Cracking: Technical Report* (The Welding Institute, 1973).

32. N. R. Quick and H. H. Johnson, "Hydrogen and Deuterium in Iron 49-506°C," *Acta Metallurgica* 26 (1978): 903–907.

33. H. K. D. H. Bhadeshia, *Theory of Transformations in Steels* (CRC Press, Taylor and Francis Group, 2021).

34. N. Nanninga, Y. Levy, E. S. Drexler, R. Condon, A. Stevenson, and A. J. Slifka, "Comparison of Hydrogen Embrittlement in Three Pipeline Steels in High Pressure Gaseous Hydrogen Environments," *Corrosion Science* 59 (2012): 1–9.

35. J. A. Ronevich, J. G. Speer, and D. K. Matlock, "Hydrogen Embrittlement of Commercially Produced Advanced High Strength Sheet Steels," *SAE International Journal of Materials and Manufacturing* 3 (2010): 255–267.

36. Y. Momotani, A. Shibata, D. Terada, and N. Tsuji, "Effect of Strain Rate on Hydrogen Embrittlement in Low-Carbon Martensitic Steel," *International Journal of Hydrogen Energy* 42 (2017): 3371–3379.

37. F. Suárez, J. C. Gálvez, D. A. Cendón, J. M. Atienza, F. Sket, and J. Molina-Aldareguia, "Analysis of the Damage Evolution in Steel Specimens Under Tension by Means of XRCT," in International Symposium on Notch Fracture (Universidad de Cantabria, 2017), 88–93.

38. H. K. D. H. Bhadeshia, *Pearlite in Steels* (Taylor & Francis (CRC Press, Routledge), 2024).

39. T. Kushida, N. Kuratomi, T. Kudoh, H. Matsumoto, T. Tsumura, and F. Nakasato, "Delayed Fracture and Hydrogen Absorption of 1.3 GPa Grade High Strength Bolt Steel," *Tetsu-to-Hagane* 82 (1996): 297–302.

40. S. Yamasaki and H. K. D. H. Bhadeshia, "Precipitation during Tempering of Fe-C-Mo-V and Relationship to Hydrogen Trapping," *Proceedings of the Royal Society of London A* 462 (2006): 2315–2330.

41. J. H. Ryu, Y. S. Chun, C. S. Lee, H. K. D. H. Bhadeshia, and D. W. Suh, "Effect of Deformation on Hydrogen Trapping and Effusion in TRIP-Assisted Steel," *Acta Materialia* 60 (2012): 4085–4092.

42. J. H. Ryu, S. K. Kim, C. S. Lee, D. W. Suh, and H. K. D. H. Bhadeshia, "Effect of Aluminium on Hydrogen-Induced Fracture Behavior in Austenitic Fe-Mn-C Steel," *Proceedings of the Royal Society A* 469 (2013): 20120458.

43. H. K. D. H. Bhadeshia, *Prevention of Hydrogen Embrittlement in Steels* (ISIJ International, 2016). 24–36, Vol. 56.

44. J. Song and W. Curtin, "A Nanoscale Mechanism of Hydrogen Embrittlement in Metals," *Acta Materialia* 59 (2011): 1557–1569.

45. J. Song and W. A. Curtin, "Atomic Mechanism and Prediction of Hydrogen Embrittlement in Iron," *Nature Materials* 12 (2013): 145–151.

46. H. Westergaard, "Bearing Pressures and Cracks: Bearing Pressures through a Slightly Waved Surface or through a Nearly Flat Part of a Cylinder, and Related Problems of Cracks," *Journal of Applied Mechanics* 6 (1939): A49–A53.

47. G. Irwin, "Analysis of Stresses and Strains near the End of a Crack Traversing a Plate," *Journal of Applied Mechanics* 24 (1957): 361–364.

48. J. Bockris, W. Beck, M. Genshaw, P. Subramanyan, and F. Williams, "The Effect of Stress on the Chemical Potential of Hydrogen in Iron and Steel," *Acta Metallurgica* 19 (1971): 1209–1218.

49. W. Song, J. Von Appen, P. Choi, R. Dronskowski, D. Raabe, and W. Bleck, "Atomic-Scale Investigation of ε and θ Precipitates in Bainite in 100Cr6 Bearing Steel by Atom Probe Tomography and Ab Initio Calculations," *Acta Materialia* 61, no. 20 (2013b): 7582–7590.

50. K. Sato, "Improving the Toughness of Ultrahigh Strength Steel," Ph.D. thesis (University of California,2002).

51. P. Marshall, *Austenitic Stainless Steels: Microstructure and Mechanical Properties* (Elsevier Applied Science Publishers, 1984).

52. M. Grujicic and X. Zhou, "Atomistic Simulation of Thermally Activated Glide of Dislocations in Fe-Ni-Cr-N Austenite," *Materials Science and Engineering: A* 190 (1995): 87–98.

53. T. Michler, C. San Marchi, J. Naumann, S. Weber, and M. Martin, "Hydrogen Environment Embrittlement of Stable Austenitic Steels," *International Journal of Hydrogen Energy* 37 (2012): 16231–16246.

54. B. Ousiabou, S. W. Ooi, V. Javaheri, and E. Ghassemali, "On Accelerated Design, and Characterization of a Hydrogen-Embrittlement Tolerant Mn-Steel," *Engineering Failure Analysis* 162 (2024): 108438.

55. Y. Fan, F. Cui, L. Lu, and B. Zhang, "A Nanotwinned Austenite Stainless Steel with High Hydrogen Embrittlement Resistance," *Journal of Alloys and Compounds* 788 (2019): 1066–1075.

56. M. Y. Panchenko, A. Nifontov, and E. Astafurova, "Microstructural Effect on Hydrogen Embrittlement of High Nitrogen Chromium-Manganese Steel," *Physical Mesomechanics* 25 (2022): 453–465.

57. V. Shivanyuk, V. Gavriljuk, and J. Foct, "Mechanism of Hydrogen Embrittlement of Austenitic Steels," *Materials Science Forum* 539 (2007): 4249–4254.

58. Q. Chen, G. Zhou, Y. Huang, and W. Chu, "Hydrogen-Inducing Nanovoids in Thin Crystals of 310 Stainless Steel," *Journal of Materials Science* 33 (1998): 4813–4819.

59. M. Hatano, M. Fujinami, K. Arai, H. Fujii, and M. Nagumo, "Hydrogen Embrittlement of Austenitic Stainless Steels Revealed by Deformation Microstructures and Strain-Induced Creation of Vacancies," *Acta Materialia* 67 (2014): 342–353.

60. L. Chiari, R. Mizukami, and T. Nishiwaki, "Hydrogen-Induced Vacancy Formation Process in Austenitic Stainless Steel 304," *ISIJ International* 65 (2025): 644–649.

61. V. Gavriljuk, V. Bugaev, Y. N. Petrov, A. Tarasenko, and B. Yanchitski, "Hydrogen-Induced Equilibrium Vacancies in FCC Iron-Base Alloys," *Scripta Materialia* 34 (1996): 903–907.

62. Y. Kong, P. Kathayat, A. Williamson, et al., "Influence of Stacking Fault Energy and Hydrogen on Deformation Mechanisms in High Mn Austenitic Steels during in-Situ Tensile Testing," *International Journal of Hydrogen Energy* 148 (2025): 149833.

63. I. Kireeva, Y. I. Chumlyakov, A. Tverskov, and H. Maier, "Effect of Hydrogen on Orientation Dependence of Critical Shear Stress and Mechanism of Straining in Single Crystals of Stable Stainless Steel," *Technical Physics Letters* 37 (2011): 522–525.

64. G. B. Olson and M. Cohen, "A General Mechanism of Martensitic Nucleation, Pt. I. General Concepts and the FCC→HCP Transformation," *Metallurgical Transactions A* 7 (1976): 1897–1904.

65. S.-I. Lee, J.-M. Lee, S.-Y. Lee, et al., "Tensile and Fracture Behaviors of Austenitic High-Manganese Steels Subject to Different Hydrogen Embrittlement Test Methods," *Materials Science and Engineering: A* 766 (2019): 138367.

66. S.-Y. Lee and B. Hwang, "Hydrogen Embrittlement of Three High-Manganese Steels Tested by Different Hydrogen Charging Methods," *Korean Journal of Metals and Materials* 55 (2017): 695–702.

67. Y.-H. Nam, J.-S. Park, U.-B. Baek, J.-Y. Suh, and S.-H. Nahm, "Low-Temperature Tensile and Impact Properties of Hydrogen-Charged High-Manganese Steel," *International Journal of Hydrogen Energy* 44 (2019): 7000–7013.

68. V. Gavriljuk, V. Shyvaniuk, and S. Teus, "Electron Concept of Hydrogen Embrittlement and Hydrogen-Increased Plasticity of Metals," *Progress in Physics of Metals/Uspehi Fiziki Metallov* 25 (2024): 482–518.

69. H. Khanchandani, D. Ponge, S. Zaefferer, and B. Gault, "Hydrogen-Induced Hardening of a High-Manganese Twinning Induced Plasticity Steel," *Materialia* 28 (2023): 101776.

70. I. B. Tu`luca, M. Koyama, B. Bal, D. Canadinc, E. Akiyama, and K. Tsuzaki, "High-Concentration Carbon Assists Plasticity-Driven Hydrogen Embrittlement in a Fe-High Mn Steel with a Relatively High Stacking Fault Energy," *Materials Science and Engineering: A* 717 (2018): 78–84.

71. I.-J. Park, S.-M. Lee, H.-H. Jeon, and Y.-K. Lee, "The Advantage of Grain Refinement in the Hydrogen Embrittlement of Fe-18Mn-0.6 C Twinning-Induced Plasticity Steel," *Corrosion Science* 93 (2015): 63–69.

72. M. Moallemi, H.-J. Cho, and S.-J. Kim, "The Adverse Effect of Grain Refinement on Hydrogen Embrittlement in a High Mn Austenitic Steel," *Materials Science and Engineering: A* 916 (2024): 147367.

73. N. Narita, C. Altstetter, and H. Birnbaum, "Hydrogen-Related Phase Transformations in Austenitic Stainless Steels," *Metallurgical Transactions A* 13 (1982): 1355–1365.

74. D. P. Abraham and C. J. Altstetter, "The Effect of Hydrogen on the Yield and Flow Stress of an Austenitic Stainless Steel," *Metallurgical and Materials Transactions A* 26 (1995a): 2849–2858.

75. D. P. Abraham and C. J. Altstetter, "Hydrogen-Enhanced Localization of Plasticity in an Austenitic Stainless Steel," *Metallurgical & Materials Transactions A* 26 (1995b): 2859–2871.

76. M. Thrun, C. Finfrock, A. Clarke, and K. Clarke, "Effects of Unloading on Subsequent Yielding Behavior in 304 Stainless Steel," *Frontiers in Materials* 7 (2021): 615361.

77. I. Gupta and J. Li, "Stress Relaxation, Internal Stress, and Work Hardening in Some Bcc Metals and Alloys," *Metallurgical Transactions* 1 (1970): 2323–2330.

78. K. Nibur, D. Bahr, and B. Somerday, "Hydrogen Effects on Dislocation Activity in Austenitic Stainless Steel," *Acta Materialia* 54 (2006): 2677–2684.

79. W. C. Oliver and G. M. Pharr, "Measurement of Hardness and Elastic Modulus by Instrumented Indentation: Advances in Understanding and Refinements to Methodology," *Journal of Materials Research* 19 (2004): 3–20.

80. H. Y. Yu and C. X. Zhou, "Elastic Modulus Model Based on Dislocation Density and Its Application on Aluminum Alloy 5052," *Key Engineering Materials* 725 (2017): 659–664.

81. E. Akiyama, "Evaluation of Delayed Fracture Property of High Strength Bolt Steels," *ISIJ International* 52 (2012): 307–315.

82. M. Wasim and T. D. Ngo, "Failure Analysis of Structural Steel Subjected to Long Term Exposure of Hydrogen," *Engineering Failure Analysis* 114 (2020): 104606.

83. B. Swieczko-Zurek, A. Zielinski, and E. Lunarska, "Hydrogen Degradation of Structural Steels in Technical Hydrocarbon Liquids," *Materials and Corrosion* 59 (2008): 289–295.

84. Y. Shi, R. He, B. Zhang, and Z. Zhong, "Revisiting the Phase Diagram and Piezoelectricity of Lead Zirconate Titanate from First Principles," *Physical Review B* 109 (2024): 174104.

85. T.-Y. Zhang, F.-X. Jiang, W.-Y. Chu, and C.-M. Hsiao, "Effect of Hydrogen on the Youngs Modulus of Iron," *Metallurgical Transactions A* 16 (1985): 1655–1662.

86. M. J. Spencer, A. Hung, I. K. Snook, and I. Yarovsky, "Density Functional Theory Study of the Relaxation and Energy of Iron Surfaces," *Surface Science* 513 (2002): 389–398.

87. A. Sieverts, “Die löslichkeit Von Wasserstoff in Kupfer, Eisen Und Nickel,” *Zeitschrift für Physikalische Chemie* 77 (1911): 591–613.

88. A. Sieverts, “Absorption of Gases by Metals,” *Zeitschrift für Metallkunde* 21 (1929): 37–46.

89. H. H. Johnson, “Hydrogen in Iron,” *Metallurgical and Materials Transactions A* 19 (1988): 691–707.